Concentration-Dependent Inhibitory Effects of Apolipoprotein E on Alzheimer's β-Amyloid Fibril Formation *in Vitro*†

Hironobu Naiki,*,‡ Fumitake Gejyo,§ and Kazuya Nakakuki‡

Department of Pathology and Department of Clinical and Laboratory Medicine, Fukui Medical School, Fukui 910-11, Japan

Received October 1, 1996; Revised Manuscript Received February 19, 1997⊗

ABSTRACT: Recently, many research groups have examined the effect of apolipoprotein E (apoE) on β-amyloid fibril (βAf) formation *in vitro*. However, their data were somewhat controversial and no exact kinetic assessment of the role of apoE has thus far been available. We examined the effect of human apoE on βAf formation *in vitro*, starting with various concentrations of freshly prepared β-amyloid(1−40) (β1−40) and using fluorescence spectroscopy with thioflavine T. When 50 μM of β1−40 was incubated with a 1:1000 to 1:100 molar ratio of apoE, a dose-dependent inhibitory effect of apoE was observed. Both the nucleation and extension phases of βAf formation *in vitro* were inhibited by apoE. On the other hand, when 300 μM of β1−40 was incubated with a 1:100 molar ratio of apoE, the inhibitory effect of apoE was completely abolished. We then focused our study on the kinetics of the inhibitory effect of apoE on the extension phase of βAf formation *in vitro*, utilizing the recently established first-order kinetic model of βAf extension *in vitro* [Naiki, H., & Nakakuki, K. (1996) *Lab. Invest. 74*, 374−383]. The mathematical treatment of the data suggests that apoE inhibits the extension of βAf *in vitro*, by making a complex with β1−40, thus eliminating free β1−40 from the reaction mixture. The equilibrium association constant with β1−40 was practically the same among the three major recombinant apoE isoforms. These results indicate that the effects of apoE on βAf formation *in vitro* is differential and could settle some of the controversy about β-amyloid-apoE interaction *in vitro*.

Apolipoprotein E (apoE)[1] is a cholesterol transport protein that serves as a ligand for low-density lipoprotein receptors (Mahley, 1988). ApoE is synthesized in various organs including the brain and is present in high concentrations in the interstitial fluid (Mahley, 1988; Poirier, 1994). In both, the central and peripheral nervous systems, apoE appears to participate in cholesterol redistribution and the repair response to tissue injury (Mahley, 1988; Poirier, 1994). Recently, several experiments have strengthened the hypothesis that apoE may play a central role in the pathogenesis of Alzheimer's disease (AD) (Poirier, 1994; Castaño et al., 1995a). First, apoE immunoreactivity was observed in cerebral β-amyloid deposits in patients with AD (Namba et al., 1991; Wisniewski & Frangione, 1992). ApoE was found to form stable complexes with β-amyloid fibrils (βAf) in AD brain tissue (Näslund et al., 1995). Second, apoE was found to form sodium dodecyl sulfate stable complexes with amyloid β-peptides (Aβ) in *in vitro* studies (Wisniewski et al., 1993b; Strittmatter et al., 1993a,b). Third, a strong genetic association has been reported between late-onset AD and the three alleles of apoE [i.e., ε2 (Cys^{112}−Cys^{158}), ε3 (Cys^{112}−Arg^{158}), and ε4 (Arg^{112}−Arg^{158})] (Strittmatter et al., 1993a; Corder et al., 1993, 1994; Schmechel et al., 1993). The risk of developing AD increases, and the mean age at onset decreases with increasing number of ε4 alleles (Strittmatter et al., 1993a; Corder et al., 1993). Moreover, the ε4 allele was found to be strongly associated with increased cerebral β-amyloid deposits (Schmechel et al., 1993). On the other hand, the ε2 allele was found to have a protective effect against late-onset AD (Corder et al., 1994).

The data described above prompted many research groups to examine the effect of apoE on βAf formation *in vitro*. Some groups reported that apoE promoted and accelerated βAf formation from Aβ *in vitro* (Wisniewski et al., 1994a; Sanan et al., 1994; Ma et al., 1994; Castaño et al., 1995b; Golabek et al., 1996). On the basis of these observations, apoE has been regarded as one of the "pathological molecular chaperones" which are the "promotors" of amyloid fibril formation from various precursor proteins (Wisniewski & Frangione, 1992; Wisniewski et al., 1994b). In contrast, other groups reported that apoE inhibited βAf formation *in vitro* (Schwarzman et al., 1994; Evans et al., 1995; Wood et al., 1996). These theories are somewhat controversial and no exact kinetic assessment of the role of apoE has thus far been available.

Recently, we and other groups proposed that a nucleation-dependent polymerization model could explain the mechanisms of βAf formation *in vitro* (Jarrett & Lansbury, 1992, 1993; Jarrett et al., 1993; Evans et al., 1995; Naiki & Nakakuki, 1996; Esler et al., 1996, Lomakin et al., 1996; Wood et al., 1996). This model consists of two phases, i.e., nucleation and extension phases. Nucleus formation requires a series of association steps of monomers that are thermodynamically unfavorable, representing the rate-limiting step

† This research was supported in part by Grant-in-Aid 08670242 for Scientific Research (C) from the Ministry of Education, Science, Sports and Culture of Japan.

* Corresponding author. Tel: 081-776-61-3111, ext 2236. Fax: 081-776-61-8123. E-mail: naiki@fmsrsa.fukui-med.ac.jp.

‡ Department of Pathology, Fukui Medical School.

§ Department of Clinical and Laboratory Medicine, Fukui Medical School.

⊗ Abstract published in *Advance ACS Abstracts,* May 1, 1997.

[1] Abbreviations: Aβ, amyloid β-peptides; AD, Alzheimer's disease; apoE, apolipoprotein E; α_1-MG, α_1-microglobulin; βAf, β-amyloid fibrils; β1−40, β-amyloid(1−40); CD, circular dichroism; CSF, cerebrospinal fluid; f(1−40), βAf formed from β1−40; ThT, thioflavine T.

S0006-2960(96)02470-1 CCC: $14.00

in amyloid fibril formation. Once the nucleus (*n*-mer) has been formed, further addition of monomers becomes thermodynamically favorable, resulting in rapid extension of amyloid fibrils. We and other groups have independently developed a first-order kinetic model of βAf extension *in vitro* by measuring the polymerization velocity of βAf as an indicator of the reaction and confirmed that the extension of βAf proceeds via the consecutive association of β-amyloid(1−40) (β1−40) onto the ends of existing fibrils (Naiki & Nakakuki, 1996; Esler et al., 1996, Lomakin et al., 1996). Although this model is based on the assumption that β1−40 is monomeric in the reaction mixture, stable Aβ dimers suggested by Soreghan et al. (1994) would also be consistent with this model.

On the basis of the above described model, and utilizing fluorescence spectroscopy with thioflavine T (ThT) (Naiki & Nakakuki, 1996), we analyzed the effect of apoE on βAf formation *in vitro*.

EXPERIMENTAL PROCEDURES

Formation of βAf from β1−40. βAf [f(1−40)] was formed from synthetic β1−40 (lot number WM365, Bachem, Torrance, CA), essentially as described elsewhere (Naiki & Nakakuki, 1996). Briefly, β1−40 was dissolved in ice-cold distilled water at a concentration of 500 μM (2.2 mg/ml). The reaction mixture was 150 μL and contained 400 μM β1−40, 100 mM NaCl, and 50 mM phosphate buffer, pH 7.5. Polymerization reactions were performed in oil-free PCR tubes (size, 0.5 mL, code number, 9046; Takara Shuzo Co. Ltd., Otsu, Japan) at 37 °C for 3 days. After incubation, 5 M NaCl was added to a final NaCl concentration of 150 mM and centrifuged at 4 °C for 90 min at 1.5×10^4 rpm, using a high-speed microrefrigerated centrifuge (MRX-150, Tomy, Tokyo, Japan). The pellet was resuspended in 100 mM NaCl, 50 mM phosphate buffer, pH 7.5, and 0.05% NaN_3, extensively sonicated on ice, and stored at 4 °C before assaying.

Fluorescence Spectroscopy. All studies were performed essentially as described elsewhere (Naiki & Nakakuki, 1996) on a Hitachi F-3010 fluorescence spectrophotometer. Optimum fluorescence measurements of f(1−40) were obtained at the excitation and emission wavelengths of 446 and 490 nm, respectively, with the reaction mixture containing 5 μM ThT (Nacalai tesque, Inc., Kyoto, Japan) and 50 mM of glycine-NaOH buffer, pH 8.5 (Naiki & Nakakuki, 1996). Fluorescence was measured immediately after making the mixture and was averaged for an initial 5 s.

Polymerization Assay. In all experiments, the volume of the reaction mixture used was 30 μL and the reactions were carried out in oil-free PCR tubes. Reaction mixtures were prepared on ice at 4 °C, with neither polymerization nor depolymerization of f(1−40) being observed by fluorometric analysis. First, distilled water was put into a tube such that the final volume of the reaction mixture would be 30 μL. Second, 500 mM phosphate buffer, pH 7.5, was added to yield a final buffer concentration of 50 mM. Third, 5 M NaCl was added to a final concentration of 100 mM. In the extension kinetics study (Figures 4−6), in order to avoid the *de novo* nucleation of β1−40, 6 M urea was added to a final concentration of 1 M. Fourth, β1−40, dissolved in ice-cold distilled water at a concentration of 1.0 (Figures 1−3) or 0.5 mM (Figures 4−6), was added to yield a final β1−40 concentration of 50, 150, and 300 μM (Figures 1−3), or 0, 20, 40, 60, 80, 100, and 120 μM (Figures 4−6). Fifth, recombinant human apoE2, E3, or E4 [lot numbers: CAF7252, LEP 7841 (E2), SKK7520, LEQ7625 (E3), and SKP7961, LEL 7273 (E4), respectively, Wako Pure Chemical Industries, Ltd., Osaka, Japan] dissolved in 50 mM phosphate buffer, pH 7.5, 100 mM NaCl (Figures 1−3) or 6 M urea (Figures 4−6) was added to yield a final apoE concentration of 0, 50, 100, 500 nM, 1, 1.5, 2, 3, and 4 μM (Figures 1−3), or 0, 200, 400, 600, 800 nM, 1, 1.2, 1.4, 1.6, 1.8, and 2 μM (Figures 4−6). Recombinant apoE was supplied at 0.42−0.65 mg/ml in 0.7 M ammonium bicarbonate. To remove ammonium bicarbonate, they were lyophilized, then dissolved in ice-cold 6 M urea at a concentration of 12 μM, to obtain all molecules in monomeric form (Figures 4−6). In order to remove urea, some of them were subsequently dialyzed against 50 mM phosphate buffer, pH 7.5, 100 mM NaCl at 4 °C (Figures 1−3). In Figure 1, human α_1-microglobulin (α_1-MG) [lot number: 065(501), DAKO A/S, Glostrup, Denmark] dissolved in 15 mM NaN_3 at a concentration of 554 mg/L (20.7 μM) was added as a negative control of apoE to a final α_1-MG concentration of 0, 500 nM, 1.5, and 3 μM. Finally, f(1−40) solution was added to yield a final f(1−40) concentration of 50 ng protein/μL (Figure 1B and Figures 4−6).

A 5 μL aliquot of each reaction mixture was initially assayed by fluorescence spectroscopy. The reaction tubes were then transferred into a DNA thermal cycler (PJ480, Perkin Elmer Cetus, Emeryville, CA). Starting at 4 °C, the plate temperature was elevated at maximal speed to 37 °C. Incubation times ranged between 0 and 24 h (as indicated in each figure), and the reaction was stopped by placing the tubes on ice. The reaction tubes were not agitated throughout the reaction. From each reaction tube, triplicate 5 μL aliquots were removed then subjected to fluorescence spectroscopy, and the mean of each triplicate was determined.

In some experiments, the reaction mixtures were centrifuged at 4 °C for 60 min at 1.5×10^4 rpm. Under these conditions, 100 ng/μL of pure f(1−40) suspended in 50 mM phosphate buffer, pH 7.5, 100 mM NaCl had all precipitated as measured by the fluorescence of ThT.

Secondary Structure Analysis. Secondary structure of β1−40 was analyzed by circular dichroism (CD). The mixture contained 25 μM β1−40 and 10 mM phosphate buffer, pH 7.5. The CD spectrum was recorded at room temperature, using a 1.0 mm path-length cell on a Jasco 720WI spectropolarimeter (Jasco corporation, Hachioji, Japan). Ten accumulative readings at 1 nm band width, resolution at 0.1 nm, sensitivity at 10 mdeg, response time of 2 s, and scan speed at 50 nm/min were taken from each sample, averaged, and base line subtracted. Results were expressed in terms of molar ellipticity (ϑ), ranged from 260 to 183 nm. The content of β-sheet structure was estimated by curve fitting using Yang's algorithm (Yang et al., 1986).

Other Analytical Procedures. Protein concentrations of the f(1−40) and apoE solutions were determined by the method of Bradford (Bradford, 1976), using a protein assay kit (500−0001, Bio-Rad Laboratories, Inc., Hercules, CA). Bovine gamma globulin was used as the standard. Linear least squares fit and general curve fit of the data were performed using KaleidaGraph (version 2.1, Synergy Software, Reading, PA) and a Macintosh computer. One-way analysis of variance was used for statistical analysis.

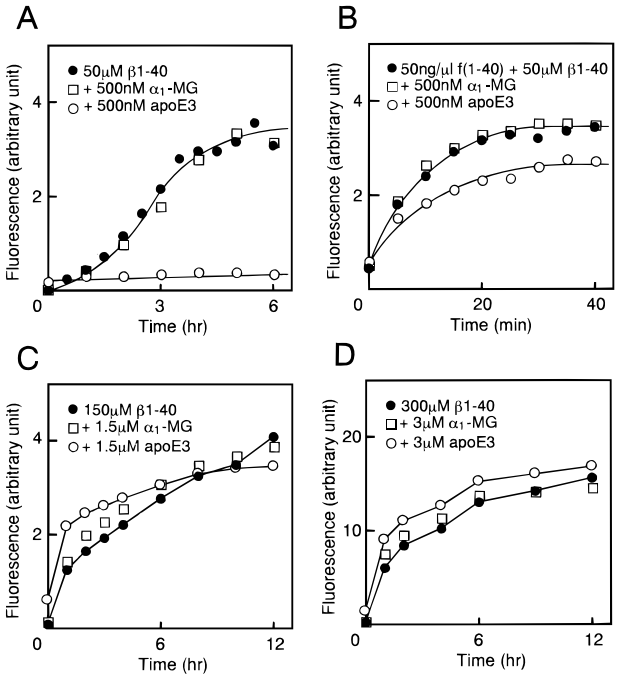

FIGURE 1: Effect of β1−40 concentration on the time course of f(1−40) formation in the presence and absence of a 1:100 molar ratio of α_1-MG or apoE3. The reaction mixture contained 50 mM phosphate buffer, pH 7.5, 100 mM NaCl, and 50 (A, B), 150 (C), and 300 μM (D) β1−40. In panel B, the reaction mixture contained 50 ng/μL f(1−40). In each experiment, a 1:100 molar ratio of α_1-MG (□) or apoE3 (○) was added to the reaction mixture, and their time courses were compared with that of β1−40 alone (●). The reaction was initiated by shifting the temperature to 37 °C, as described under Experimental Procedures. At each incubation time (0 to 12 h), the reaction of the corresponding tube was stopped and analyzed by fluorescence spectroscopy as described under Experimental Procedures. Each panel is a representative pattern of at least three independent experiments.

RESULTS

Differential Effects of apoE on βAf Formation in vitro. We first analyzed the secondary structure of β1−40, used in the present study, by CD. From the CD spectra, which had a negative peak near 199 nm (data not shown), the content of β-sheet structure was estimated to be 44.5%.

As shown in Figure 1A, when 50 μM of freshly prepared β1−40 was incubated at 37 °C, the fluorescence of ThT followed a characteristic sigmoidal curve, i.e., an initial lag phase, a subsequent growth phase, and a final equilibrium phase. This curve is consistent with a nucleation-dependent polymerization model, and the first two phases correspond to nucleation and extension phases (Jarrett & Lansbury, 1992, 1993; Jarrett et al., 1993; Evans et al., 1995). This process was completely inhibited by 500 nM (1:100 molar ratio) apoE3. When 50 μM β1−40 was incubated with 50 ng/μL of f(1−40) at 37 °C, the fluorescence increased without a lag phase and proceeded to equilibrium within 30 min (Figure 1B). In this process, called "seeding", the nucleation phase is skipped and the elongation phase emerges immediately after initiation of the reaction, because of the presence of preformed nuclei [i.e., f(1−40)] (Jarrett & Lansbury, 1993). Again, this process was partly inhibited by 500 nM of apoE3.

As shown in Figure 1D, when 300 μM β1−40 was incubated at 37 °C, a hyperbolic curve without a lag phase was obtained. This process was not inhibited by 3 μM (1:100 molar ratio) apoE3. On the contrary, a slight upward shift of the hyperbolic curve was observed in the presence of apoE. At 1 h postinitiation, the presence of apoE3 had caused a 1.5-fold increase in fluorescence.

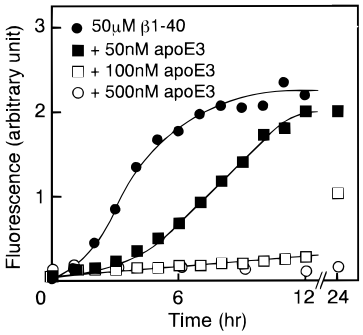

FIGURE 2: Effect of apoE3 concentration on the time courese of f(1−40) formation from 50 μM β1−40. The reaction mixture contained 50 μM β1−40, 50 mM phosphate buffer, pH 7.5, 100 mM NaCl, and 0 (●), 50 (1:1000) (■), 100 (1:500) (□), and 500 nM (1:100) (○) apoE3. The reaction was initiated by shifting the temperature to 37 °C, as described under Experimental Procedures. At each incubation time (0 to 24 h), the reaction of the corresponding tube was stopped and analyzed by fluorescence spectroscopy as described under Experimental Procedures. This is a representative pattern of three independent experiments.

When the β1−40 concentration was 150 μM, the effect of adding apoE3 at a 1:100 molar ratio was biphasic (Figure 1C), i.e., in the early phase of the reaction, the presence of apoE3 caused an increase in fluorescence, while in the late phase, it effected a slight decrease in fluorescence.

α_1-MG had no significant effect on the above described time course experiments. Both apoE2 and E4 had similar differential effects on f(1−40) formation *in vitro* (data not shown).

Next, the dose dependency of the above described differential effects of apoE3 was analyzed. When 50 μM β1−40 was incubated with increasing concentrations of apoE3, a dose-dependent elongation of the lag phase was observed (Figure 2). In the equilibrium phase of Figures 1B and 2, all of the fluorescence precipitated after centrifugation and equal protein concentrations of the pellet suspensions gave similar fluorescence regardless of the presence or absence of apoE3 (data not shown). Moreover, electron microscopic study showed that βAf formed in the presence or absence of apoE3 is indistinguishable (data not shown). Evans et al. (1995) also reported that amyloid fibrils formed in the presence of inhibitory concentrations of apoE3 and E4 were indistinguishable from those formed in their absence, with regard to their morphology (electron microscopy) and secondary structure (Fourier transform infrared microscopy).

When 300 μM β1−40 was incubated with increasing concentrations of apoE3, a dose-dependent increase in the fluorescence, before and 1 h after initiation of the reaction, was observed (Figure 3). In both cases, the fluorescence increased linearly with the concentration of apoE3. In a typical precipitation experiment of the mixture containing 300 μM β1−40 and 3 μM apoE3, 75% of the fluorescence was soluble before the reaction, while 80 and 95% of the fluorescence precipitated at 1 and 24 h postinitiation of the reaction, respectively. At 24 h postinitiation, equal protein concentrations of the pellet suspensions gave similar fluorescence regardless of the presence or absence of apoE3 (data not shown).

Kinetics of the Inhibitory Effect of apoE on the Extension Phase of f(1−40) Formation in Vitro. We then focused our

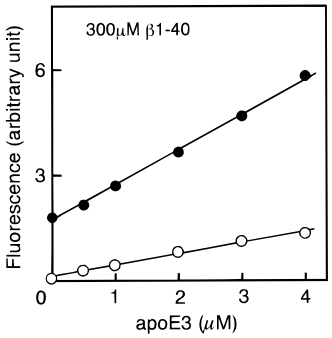

FIGURE 3: Effect of apoE3 concentration on the initial phase of f(1−40) formation from 300 μM β1−40. The reaction mixture contained 300 μM β1−40, 50 mM phosphate buffer, pH 7.5, 100 mM NaCl, and indicated concentrations of apoE3. The reaction was carried out for 1 h at 37 °C, as described under Experimental Procedures and the fluorescence before (○) and after (●) the reaction was plotted. Linear least squares fit was performed (r = 0.995 and 0.999 for ○ and ●, respectively). This is a representative pattern of three independent experiments.

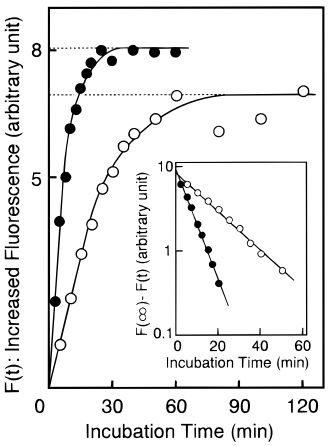

FIGURE 4: Time course of the fluorescence increase after the initiation of the extension reaction in the presence (○) and absence (●) of apoE3. F(t) represents the increased fluorescence as a function of time. The reaction mixture contained 120 μM β1−40, 50 ng/μL f(1−40), 50 mM phosphate buffer, pH 7.5, 100 mM NaCl, 1 M urea and 0 (●) or 400 nM (○) apoE3. The reaction was initiated by shifting the temperature to 37 °C, as described under Experimental Procedures. At each incubation time (2.5−120 min), the reaction of the corresponding tube was stopped and analyzed by fluorescence spectroscopy as described under Experimental Procedures. The inset shows the semilogarithmical plots of the difference: F(∞) − F(t) versus incubation time in both cases. F(∞) was tentatively determined and shown as a dotted line on each hyperbolic curve. Linear least-squares fit was performed for each straight line (r = −0.997 in both cases). This is a representative pattern of three independent experiments.

study on the kinetics of the inhibitory effect of apoE on the extension phase of f(1−40) formation *in vitro*, utilizing the recently established first-order kinetic model (Naiki & Nakakuki, 1996). This experimental system is designed to analyze the extension phase of βAf formation *in vitro*, in conditions where *de novo* seed formation does not occur, and measure the polymerization velocity of βAf as an indicator of the reaction.

As shown in Figure 4, when β1−40 was incubated with f(1−40) in the presence or absence of apoE3, the fluorescence increased without a lag phase and proceeded to equilibrium. A linear increase in the fluorescence was observed over 5 min in both cases. Therefore, in subsequent experiments, a fluorescence increase, 5 min after the initiation

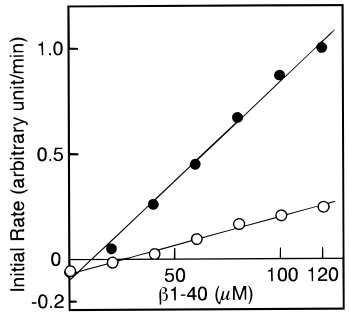

FIGURE 5: Effect of β1−40 concentration on the initial rate of f(1−40) extension in the presence (○) and absence (●) of apoE3. The reaction mixture contained 50 ng/μL f(1−40), 50 mM phosphate buffer, pH 7.5, 100 mM NaCl, 1M urea, 0 (●) or 400 nM (○) apoE3 and indicated concentrations of β1−40. The reaction was carried out for 5 min at 37 °C, as described under Experimental Procedures and the increased fluorescence was regarded as the initial rate of extension. Linear least-squares fit was performed for each straight line (r = 0.996 and 0.997 for ○ and ●, respectively). This is a representative pattern of four independent experiments.

of the reaction, was taken as the initial rate of extension. In the presence of apoE3, both the initial rate and the equilibrium level were lower than those observed in the absence of apoE3. In the equilibrium phase, all of the fluorescence precipitated after the centrifugation and equal protein concentrations of the pellet suspensions gave similar fluorescence regardless of the presence or absence of apoE3 (data not shown). β1−40 incubated without f(1−40) at 37 °C showed no increase in the fluorescence over a 120 min reaction time regardless of the presence or absence of apoE (data not shown).

Plotting the fluorescence data as common logarithms, shown as an inset, gives two perfect linear semilogarithmical plots (r = −0.997 in both cases). Interpretation of these plots yields the following equation:

$$\log[A - F(t)] = a - bt \qquad (1)$$

where t is the reaction time, $F(t)$ is the increased fluorescence as a function of time, A is tentatively determined as $F(\infty)$, a and $-b$ are the y-intercept and the slope of each straight line, respectively. Differentiating eq 1 by t and subsequent rearrangement yields the following differential equation:

$$F'(t) = B - CF(t) \qquad (2)$$

where $B = bA \ln 10$, $C = b \ln 10$, and $F'(t)$ represents the rate of fluorescence increase at a given time. The differences in A and $-b$ between two straight lines will be discussed later.

At a constant f(1−40) concentration, a good linearity was observed between the β1−40 concentration and the initial rate of f(1−40) extension in both the presence and the absence of apoE3 (Figure 5). This linearity indicates that (1) the initial rate of polymerization is proportional to the β1−40 concentration and (2) at each β1−40 concentration, the net rate of f(1−40) extension is the sum of the rates of polymerization and depolymerization (Naiki & Nakakuki, 1996). In the presence of apoE3, the slope of the straight line decreased, without changing the y-intercept.

At a constant β1−40 concentration, the initial rate decreased exponentially as the apoE3 concentration increased (Figure 6). At 2 μM apoE3, a negative initial rate was observed. When these data points were applied to function

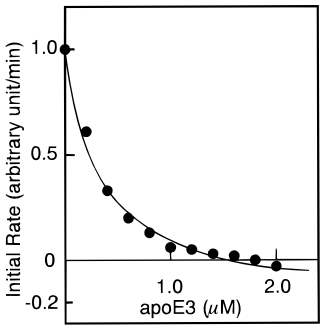

FIGURE 6: Effect of apoE3 concentration on the initial rate of f(1−40) extension. The reaction mixture contained 120 μM β1−40, 50 ng/μL f(1−40), 50 mM phosphate buffer, pH 7.5, 100 mM NaCl, 1 M urea, and indicated concentrations of apoE3. The reaction was carried out for 5 min at 37 °C, as described under Experimental Procedures, and the increased fluorescence was regarded as the initial rate of extension. The data points were fitted to the function 3 described in the text ($r = -0.996$). This is a representative pattern of three independent experiments.

Table 1. Effect of apoE Isoforms on the Kinetic Parameters of the Inhibitory Effect of apoE

	kinetic parameters	
isoforms	K_i[a](m[b]) (μM)	$-k_{-1}$[P][a] (n[b]) (arbitrary unit/min)
apoE2	0.37 ± 0.07[c]	−0.25 ± 0.05[c]
apoE3	0.37 ± 0.03	−0.25 ± 0.03
apoE4	0.39 ± 0.08	−0.25 ± 0.04

[a] For details, see the legend of Figure 7 and discussion. [b] Two constant values calculated from the fitting of the data points in Figure 6 to the function 3 described in the text. [c] Means ± SE of three independent experiments. These two parameters were not significant among three isoforms (one-way ANOVA).

3 described below, a good fit was observed ($r = -0.996$).

$$Y = \frac{m + nX}{m + X} \tag{3}$$

The two constants m and n were calculated to be 0.34 and −0.21, respectively. Similar data were obtained with apoE2 and apoE4 (Table 1).

DISCUSSION

The above results indicate that the effects of apoE on βAf formation *in vitro* is differential, i.e., at low concentrations of β1−40 (50 μM), a dose-dependent inhibitory effect of apoE on f(1−40) formation *in vitro* was observed, while at high concentrations of β1−40 (300 μM), an inhibitory effect of apoE was completely abolished.

Evans et al. (1995) reported the inhibitory effect of apoE on f(1−40) formation *in vitro*, starting with a relatively low concentration (80 μM) of β1−40. In their study, a characteristic sigmoidal turbidity curve (as in Figure 1A) was observed during the incubation of β1−40, and apoE elongated the lag phase of this curve (Evans et al., 1995). Other investigators reported a stimulatory effect of apoE on f(1−40) formation starting with relatively high concentrations of β1−40: 250 μM (Wisniewski et al., 1994a), 300 μM (Castaño et al., 1995b), and 231 μM (1 mg/mL) (Golabek et al., 1996). In these studies, hyperbolic curves of ThT fluorescence (as in Figure 1D) were observed during the incubation, and apoE shifted those curves upward. In our study, this effect of apoE was very small relative to the total fluorescence intensity (see Figure 1D). As Golabek et al. (1996) showed, the fibrillogenesis of β1−40 with an initial high β-sheet content (e.g., 65.7% in B1−40, a lot used in their study) is not significantly affected by the presence of apoE. Chan et al. (1996) performed quantitation of soluble complex formation between apoE and Aβ under native conditions. They suggested that (a) apoE forms a tetramer and each apoE subunit possesses a single binding site for Aβ, which mediates rapid complex formation to yield a 4:1 stoichiometry of β1−40 to apoE tetramer; (b) gradually soluble, higher molecular weight complexes are formed containing stoichiometries of over 100:1; and (c) these complexes superaggregate and precipitate. They reported that these coaggregates bind ThT as effectively as βAf but are extremely inefficient seeds of βAf growth. In our study, dose-dependent increase in fluorescence was observed in the preincubation mixture containing 300 μM β1−40 and 0−4 μM apoE3 (see Figure 3). Moreover, about 75% of the fluorescence remained soluble after centrifugation of the mixture containing 300 μM β1−40 and 3 μM apoE3. Thus, it may be reasonable to consider that the increased fluorescence induced at high [β1−40] (300 μM), by increasing [apoE] (0−4 μM) (see Figures 1D and 3), may be largely due to the formation of apoE-β1−40 coaggregates and not to the promotion of f(1−40) formation.

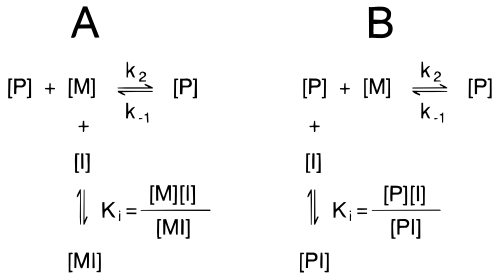

FIGURE 7: Two kinetic schemes of the inhibitory effect of apoE on f(1−40) extension. [P] is the number concentration of seed fibrils, [M] is the concentration of β1−40, k_2 and k_{-1} are the apparent rate constants for polymerization and depolymerization, respectively. [I] is the concentration of apoE, [MI] and [PI] are the concentrations of β1−40−apoE and f(1−40)−apoE complex, respectively. K_i is the equilibrium association constant for β1−40−apoE or f(1−40)−apoE complex. For details, see Discussion.

We then analyzed the kinetic properties of the inhibitory effect of apoE on f(1−40) extension *in vitro*, based on the two kinetic schemes described in Figure 7, panels A and B. We first considered a kinetic scheme as described in Figure 7A. If t is the reaction time, $f(t)$ is the concentration of β1−40, which has newly polymerized into f(1−40) during the reaction, and $[M]_0$ is the initial β1−40 concentration, then Figure 7A can be written as:

$$f'(t) = k_2[P][M] - k_{-1}[P] \tag{4}$$

$$[M] = [M]_0 - f(t) - [MI] \tag{5}$$

$$[MI] = \frac{[I]}{K_i}[M] \tag{6}$$

where $f'(t)$ represents the rate of f(1−40) extension at a given time, $k_2[P][M]$ and $-k_{-1}[P]$ denote the rate of polymerization and depolymerization, respectively. Equation 6 is based on the assumption that the association of β1−40−apoE complex is always in equilibrium. The insertion of eq 6 into eq 5 and subsequent rearrangement yields the following formula:

$$[\mathrm{M}] = \frac{1}{\psi}([\mathrm{M}]_0 - f(t)) \tag{7}$$

where

$$\psi = 1 + \frac{[\mathrm{I}]}{K_\mathrm{i}}$$

The insertion of eq 7 into eq 4 yields the following formula:

$$f'(t) = \frac{k_2}{\psi}([\mathrm{M}]_0 - f(t))[\mathrm{P}] - k_{-1}[\mathrm{P}] \tag{8}$$

If $t = 0$, then $f(0) = 0$. Therefore, from equation 8,

$$f'(0) = \frac{k_2}{\psi}[\mathrm{M}]_0[\mathrm{P}] - k_{-1}[\mathrm{P}] \tag{9}$$

This equation explains Figure 5, i.e., the slope of the straight line decreases according to ψ (thus [I]), without changing the *y*-intercept.

The rearrangement of eq 8 yields the following formula:

$$f'(t) = D - Ef(t) \tag{10}$$

where

$$D = \left(\frac{k_2}{\psi}[\mathrm{M}]_0 - k_{-1}\right)[\mathrm{P}], \quad E = \frac{k_2}{\psi}[\mathrm{P}]$$

Equation 10 is the same as eq 2 (see above), and comparison of the constants *C* and *E* explains the inset in Figure 4, i.e., the slope of the straight line decreases according to ψ (thus [I]).

If $t \rightarrow \infty$, then $f(t) \rightarrow A$, and $f'(t) \rightarrow 0$ (see Figure 4). Therefore, from eq 8, the equilibrium β1−40 concentration (critical concentration) $[\mathrm{M}]_\mathrm{e}$ is obtained.

$$[\mathrm{M}]_\mathrm{e} = [\mathrm{M}]_0 - A = \psi\frac{k_{-1}}{k_2} \tag{11}$$

Thus, $[\mathrm{M}]_\mathrm{e}$ is linear to ψ.

This equation explains the decrease in the equilibrium level (Figures 1B and 4) as well as the shift to the right of the *x*-intercept (i.e., $[\mathrm{M}]_\mathrm{e}$) (Figure 5) in the presence of apoE3.

Next, we consider the relationship between $f'(0)$ and [I]. Rearrangement of eq 9 yields the following formula:

$$f'(0) = \frac{K_\mathrm{i}(k_2[\mathrm{P}][\mathrm{M}]_0 - k_{-1}[\mathrm{P}]) - k_{-1}[\mathrm{P}][\mathrm{I}]}{K_\mathrm{i} + [\mathrm{I}]} \tag{12}$$

If $f'(0)$ in the case of $[\mathrm{I}] = 0$ is arbitrarily determined to be 1 arbitrary unit/min, then eq 12 can be rewritten as

$$f'(0) = \frac{K_\mathrm{i} + (-k_{-1}[\mathrm{P}])[\mathrm{I}]}{K_\mathrm{i} + [\mathrm{I}]} \tag{13}$$

This equation is the same as eq 3 (see above), and the two constants *m* and *n* in eq 3 represent K_i and $-k_{-1}[\mathrm{P}]$ (depolymerization rate), respectively. As shown in Table 1, K_i and $-k_{-1}[\mathrm{P}]$ of apoE isoforms (apoE2, E3, and E4) were the same.

Other groups suggested that apoE may inhibit the fibril extension by binding at or the near the extension sites of preformed fibrils and possibly the binding site of β1−40 on the emerging nuclei (Evans et al., 1995, Wood et al., 1996). Therefore, we considered another kinetic scheme as described in Figure 7B. Equations corresponding to eqs 9, 10, 11, and 13, respectively, are described as follows:

$$f'(0) = \frac{k_2}{\psi}[\mathrm{M}]_0[\mathrm{P}]_0 - \frac{k_{-1}}{\psi}[\mathrm{P}]_0 \tag{14}$$

where $[\mathrm{P}]_0$ is the initial concentration of free seed fibrils.

$$f'(t) = D' - E'f(t) \tag{15}$$

where

$$D' = \frac{1}{\psi}(k_2[\mathrm{M}]_0 - k_{-1})[\mathrm{P}]_0, \quad E' = \frac{k_2}{\psi}[\mathrm{P}]_0$$

$$[\mathrm{M}]_\mathrm{e} = [\mathrm{M}]_0 - A = \frac{k_{-1}}{k_2} \tag{16}$$

$$f'(0) = \frac{K_\mathrm{i}}{K_\mathrm{i} + [\mathrm{I}]} \tag{17}$$

This scheme cannot explain neither the increase in $[\mathrm{M}]_\mathrm{e}$ nor the decrease in the equilibrium level of the extension reaction relative to the increase in [I] (see eq 16, where $[\mathrm{M}]_\mathrm{e}$ is constant). Moreover, eq 17 fits the data points in Figure 6 less well than eq 13 ($r = -0.964$ vs -0.996).

All of the above-mentioned interpretations may indicate that a kinetic scheme as described in Figure 7A is able to explain our data more appropriately than the scheme described in Figure 7B.

Figure 7A indicates that apoE affects the thermodynamic equilibrium of β1−40 (see eq 11). As shown in Figures 1B and 4, the final equilibrium level was lower in the presence of apoE as compared to in the absence of apoE. In several time-course experiments carried out by other groups (Evans et al., 1995; Wood et al., 1996), the steepest growth rate as well as the final equilibrium level seem to decrease, in a dose-dependent manner, with apoE, suggesting that apoE might, at least in part, affect the thermodynamic equilibrium.

Wood et al. (1996) proposed a kinetic scheme described in Figure 7B, based on the following two criteria: (a) the inhibitory effect of apoE would be dose dependent and (b) higher levels of seedeing require higher levels of apoE to achieve a given delay time to reaction onset. Equations 14 and 9 indicate that both criteria could be applied not only to a kinetic scheme as described in Figure 7B but also to that described in Figure 7A.

Although Chan et al. (1996) proposed a model consistent with Figure 7B in which apoE and apoE-Aβ coaggregates selectively recruit newly formed nuclei from solution, thereby reducing their ability to initiate fibril growth, rapid formation of β1−40−apoE tetramer complexes with a 4:1 stoichiometry would be consistent with a scheme described in Figure 7A. As for the nucleation phase, it might also be reasonable to assume that apoE inhibits it by a mechanism in which apoE tetramers as well as apoE-β1−40 complexes selectively recruit free β1−40 from solution, thereby reducing their ability to form seeds *de novo*. The extension phase of f(1−40) formation *in vitro* follows a first-order kinetics, i.e., the extension rate is proportional to [β1−40] (Naiki & Nakakuki, 1996; Esler et al., 1996). On the other hand, it has been

hypothesized that the nucleation phase would have a concentration dependence of $[\beta 1-40]^n$, where n is the number of $\beta 1-40$ needed to form the minimal nucleus (Jarrett & Lansbury, 1993). Thus, if it is hypothesized that apoE inhibits the nucleation phase by the same mechanism as the elongation phase (i.e., trapping of free $\beta 1-40$ by apoE tetramers as well as by apoE-$\beta 1-40$ complexes), then small alterations in free $\beta 1-40$ concentration would have a much larger effect on the nucleation phase than on the elongation phase. Indeed, our data indicate that apoE inhibits the nucleation phase more effectively than the elongation phase (compare Figures 1, panels A and B, 2, and 6). It seems likely that both kinetic schemes in Figure 7 could explain the inhibitory effect of apoE on βAf extension *in vitro*.

In the extension kinetics study (Figures 4−6), urea was used at a final concentration of 1 M in order to avoid *de novo* nucleation of $\beta 1-40$. During the extension reaction, f(1−40) preserved the classical morphologic criteria of amyloid fibrils (i.e., the nonbranched, helical filament structure of approximately 7 nm width with a helical periodicity of approximately 120 nm and orange-green birefringence under polarized light after Congo red staining) (Naiki & Nakakuki, 1996). This may indicate that, although 1 M urea does alter the secondary structure of free $\beta 1-40$, thereby preventing *de novo* nucleation of $\beta 1-40$, binding capacity of $\beta 1-40$ to growing fibril ends is maintained and final conformation of $\beta 1-40$, when incorporated into f(1−40), is identical regardless of the presence or absence of 1 M urea. In Figure 5, a negative *y*-intercept [i.e., the depolymerization of f(1−40)] was observed in the absence of $\beta 1-40$. We observed a similar negative *y*-intercept regardless of the presence or absence of 1 M urea (data not shown). It seems likely that this negative *y*-intercept may reflect the depolymerization of f(1−40) toward the equilibrium between f(1−40) and $\beta 1-40$, rather than the denaturing effect of 1 M urea.

It has been reported that 0.7 M guanidine-HCl causes a denaturing transition in the carboxyl-terminal domain of apoE and simultaneous dissociation of apoE tetramers, while a denaturing transition in the amino-terminal domain does not occur until guanidine-HCl concentration reaches 2.4 M (Wetterau et al., 1988). Evans et al. (1995) reported that the inhibitory activity of a 22 kDa amino-terminal fragment on f(1−40) formation *in vitro* is comparable to the native apoE, while a 10 kDa carboxyl-terminal fragment has no inhibitory activity. Thus, it may be reasonable to assume that 1 M urea does not affect the conformational integrity of the amino-terminal domain nor the inhibitory activity of apoE on f(1−40) formation *in vitro*. In fact, the inhibitory potential of apoE on f(1−40) extension *in vitro* was similar regardless of the presence or absence of 1 M urea, which also indicates that 1 M urea does not affect the binding affinity between $\beta 1-40$ and apoE (compare Figures 1B and 4).

Recently, it has been shown that the rate of βAf formation from Aβ, the neurotoxic activity of Aβ, as well as the interaction of Aβ with apoE are dependent on the initial conformation of Aβ (Soto et al., 1995; Simmons et al., 1994; Golabek et al., 1996). From the estimated content of β-sheet structure (44.5%), the lot of $\beta 1-40$ used in the present study seems to have an intermediate potential of βAf formation *in vitro*, as compared to the various lots used in the above mentioned literatures.

From the kinetic analysis, K_i values of the apoE−$\beta 1-40$ complex were calculated to be in the range 0.37−0.39 μM (see Figure 7 and Table 1). Golabek et al. (1996) analyzed the binding characteristics of apoE to $\beta 1-40$ using solid phase binding studies. They quantitated the binding of solubilized apoE to $\beta 1-40$ (lot number C1−40) immobilized in microtiter plates and calculated the K_D value to be 20 nM, about one $^1/_{20}$ of our K_i values. They also examined the competitive inhibition of the above-described binding using various $\beta 1-40$ lots solubilized in the reaction mixture. The IC_{50} of C1−40 was calculated to be 2.86 μM. From a K_D of 20 nM, an IC_{50} of 2.86 μM and an initial apoE concentration of 150 nM, we calculated the K_i value of apoE−C1−40 complex to be 0.44 μM. This is a kinetic value derived from the interaction of two solubilized molecules and is similar to our own K_i values. Golabek et al. (1996) clearly indicated a strong negative correlation of an IC_{50} value with the amount of β-sheet content among various $\beta 1-40$ lots, e.g., the amount of β-sheet content, IC_{50}, and K_i values of C1−40 and B1−40 (another lot used in their study) were 13.8 and 65.7%, 2.86 and 1.43 μM, and 0.44 and 0.22 μM, respectively. Interestingly, the amount of β-sheet content and the K_i value of $\beta 1-40$ used in our study plotted between those of C1−40 and B1−40 (44.5 vs 13.8 and 65.7%, 0.37 vs 0.44 and 0.22 μM). Therefore, it seems reasonable that there may be a discrepancy between K_D (derived from a physical binding of solubilized and immobilized molecules) and K_i (derived from a kinetic interaction of two solubilized molecules), under certain experimental conditions.

The physiological concentration of Aβ in cerebrospinal fluid (CSF) was reported to be on the order of 1−2 nM (Seubert et al., 1992), about $10^{-4}-10^{-5}$ times less concentrated when compared to the concentration of $\beta 1-40$ used in our experiment (20−300 μM). The thermodynamic solubility of $\beta 1-40$ is reported to be on the order of 6−9 μM (Jarret et al., 1993). This indicates that the reaction mixtures analyzed in our experiments are supersaturated and phenomena described in this article do not happen at physiological concentrations (1−2 nM) *in vitro*. However, Esler et al. (1996) reported that a first-order kinetic model is able to explain the extension phase of f(1−40), even at the physiological concentrations of $\beta 1-40$ ($10^{-11}-10^{-7}$ M). Thus, from the data presented in this article, it may be reasonable to consider apoE to be a physiological inhibitor of βAf formation *in vivo*. Interestingly, K_i values of apoE isoforms (Table 1) were within the range of apoE concentration in the CSF obtained from healthy individuals as well as from patients with neurological disorders (i.e., 100−500 nM) (Carlsson et al., 1991). Consistent with the above scenario, CSF from healthy individuals as well as from AD patients has been found to inhibit βAf formation *in vitro* (Wisniewski et al., 1993a). Moreover, Whitson et al. (1994) reported that in hippocampal cultures, rabbit apoE attenuated the neurotoxic effect of $\beta 1-40$. This neuroprotective effect of apoE may be due to the elimination of free $\beta 1-40$ from the culture medium as a result of the formation of a complex with $\beta 1-40$, which also inhibits the formation of f(1−40) *in vitro*.

Our present study was unable to confirm a genetic association between late-onset AD and the three alleles of apoE, i.e., all three isoforms (apoE2, E3, and E4) had similar differential effects on f(1−40) formation *in vitro*, as well as similar K_i values with $\beta 1-40$. However, some indirect

effects through the lipid metabolism (Poirier, 1994), as well as some qualitative differences among the apoE isoforms (Nathan et al., 1994; Strittmatter et al., 1994), may be important in the pathogenesis of AD.

Two kinetic models described in Figure 7 clearly indicate a general pharmacological principle that could be applied to inhibit or retard amyloid fibril formation in several human amyloidoses. We believe that the experimental system described in this article may prove useful in the development of nonpeptide inhibitors of amyloid fibril formation *in vivo*.

ACKNOWLEDGMENT

We thank Dr. S. Yoshida, Department of Physiology, Fukui Medical School, for helpful experimental advice; Dr. T. Takakuwa, Jasco corporation, for CD analysis; C. Masuda, H. Okada, and N. Takimoto for excellent technical assistance; and Drs. S. P. Fairchild, Department of Pathology, O. A. Rosenwasser, and K. Tomonari, Department of Immunology, Fukui Medical School, for critical reading of the manuscript.

REFERENCES

Bradford, M. M. (1976) *Anal. Biochem. 72*, 248−254.
Carlsson, J., Armstrong, V. W., Reiber, H., Felgenhauer, K., & Seidel, D. (1991) *Clin. Chim. Acta 196*, 167−176.
Castaño, E. M., Prelli, F. C., & Frangione, B. (1995a) *Lab. Invest. 73*, 457−460.
Castaño, E. M., Prelli, F., Wisniewski, T., Golabek, A., Kumar, R. A., Soto, C., & Frangione, B. (1995b) *Biochem. J. 306*, 599−604.
Chan, W., Fornwald, J., Brawner, M., & Wetzel, R. (1996) *Biochemistry 35*, 7123−7130.
Corder, E. H., Saunders, A. M., Strittmatter, W. J., Schmechel, D. E., Gaskell, P. C., Small, G. W., Roses, A. D., Haines, J. L., & Pericak-Vance, M. A. (1993) *Science 261*, 921−923.
Corder, E. H., Saunders, A. M., Risch, N. J., Strittmatter, W. J., Schmechel, D. E., Gaskell, P. C., Jr., Rimmler, J. B., Locke, P. A., Conneally, P. M., Schmader, K. E., Small, G. W., Roses, A. D., Haines, J. L., & Pericak-Vance, M. A. (1994) *Nat. Genet. 7*, 180−184.
Esler, W. P., Stimson, E. R., Ghilardi, J. R., Vinters, H. V., Lee, J. P., Mantyh, P. W., & Maggio, J. E. (1996) *Biochemistry 35*, 749−757.
Evans, K. C., Berger, E. P., Cho, C.-G., Weisgraber, K. H., & Lansbury, P. T., Jr. (1995) *Proc. Natl. Acad. Sci. U.S.A. 92*, 763−767.
Golabek, A. A., Soto, C., Vogel, T., & Wisniewski, T. (1996) *J. Biol. Chem. 271*, 10602−10606.
Jarrett, J. T., & Lansbury, P. T., Jr. (1992) *Biochemistry 31*, 12345−12352.
Jarrett, J. T., & Lansbury, P. T., Jr. (1993) *Cell 73*, 1055−1058.
Jarrett, J. T., Berger, E. P., & Lansbury, P. T., Jr. (1993) *Biochemistry 32*, 4693−4697.
Lomakin, A., Chung, D. S., Benedek, G. B., Kirschner, D. A., & Teplow, D. B. (1996) *Proc. Natl. Acad. Sci. U.S.A. 93*, 1125−1129.
Ma, J., Yee, A., Brewer, H. B., Jr., Das, S., & Potter, H. (1994) *Nature 372*, 92−94.
Mahley, R. W. (1988) *Science 240*, 622−630.
Naiki, H., & Nakakuki, K. (1996) *Lab. Invest. 74*, 374−383.
Namba, Y., Tomonaga, M., Kawasaki, H., Otomo, E., & Ikeda, K. (1991) *Brain Res. 541*, 163−166.
Näslund, J., Thyberg, J., Tjernberg, L. O., Wernstedt, C., Karlström, A. R., Bogdanovic, N., Gandy, S. E., Lannfelt, L., Terenius, L., & Nordstedt, C. (1995) *Neuron 15*, 219−228.
Nathan, B. P., Bellosta, S., Sanan, D. A., Weisgraber, K. H., Mahley, R. W., & Pitas, R. E. (1994) *Science 264*, 850−852.
Poirier, J. (1994) *Trends Neurosci. 17*, 525−530.
Sanan, D. A., Weisgraber, K. H., Russell, S. J., Mahley, R. W., Huang, D., Saunders, A., Schmechel, D., Wisniewski, T., Frangione, B., Roses, A. D., & Strittmatter, W. J. (1994) *J. Clin. Invest. 94*, 860−869.
Schmechel, D. E., Saunders, A. M., Strittmatter, W. J., Crain, B. J., Hulette, C. M., Joo, S. H., Pericak-Vance, M. A., Goldgaber, D., & Roses, A. D. (1993) *Proc. Natl. Acad. Sci. U.S.A. 90*, 9649−9653.
Schwarzman, A. L., Gregori, L., Vitek, M. P., Lyubski, S., Strittmatter, W. J., Enghilde, J. J., Bhasin, R., Silverman, J., Weisgraber, K. H., Coyle, P. K., Zagorski, M. G., Talafous, J., Eisenberg, M., Saunders, A. M., Roses, A. D., & Goldgaber, D. (1994) *Proc. Natl. Acad. Sci. U.S.A. 91*, 8368−8372.
Seubert, P., Vigo-Pelfrey, C., Esch, F., Lee, M., Dovey, H., Davis, D., Sinha, S., Schlossmacher, M., Whaley, J., Swindlehurst, C., McCormack, R., Wolfert, R., Selkoe, D., Lieberburg, I., & Schenk, D. (1992) *Nature 359*, 325−327.
Simmons, L. K., May, P. C., Tomaselli, K. J., Rydel, R. E., Fuson, K. S., Brigham, E. F., Wright, S., Lieberburg, I., Becker, G. W., Brems, D. N., & Li, W. Y. (1994) *Mol. Pharmacol. 45*, 373−379.
Soreghan, B., Kosmoski, J., & Glabe, C. (1994) *J. Biol. Chem. 269*, 28551−28554.
Soto, C., Castaño, E. M., Kumar, R. A., Beavis, R. C., & Frangione, B. (1995) *Neurosci. Lett. 200*, 105−108.
Strittmatter, W. J., Saunders, A. M., Schmechel, D., Pericak-Vance, M., Enghild, J., Salvesen, G. S., & Roses, A. D. (1993a) *Proc. Natl. Acad. Sci. U.S.A. 90*, 1977−1981.
Strittmatter, W. J., Weisgraber, K. H., Huang, D. Y., Dong, L.-M., Salvesen, G. S., Pericak-Vance, M., Schmechel, D., Saunders, A. M., Goldgaber, D., & Roses, A. D. (1993b) *Proc. Natl. Acad. Sci. U.S.A. 90*, 8098−8102.
Strittmatter, W. J., Weisgraber, K. H., Goedert, M., Saunders, A. M., Huang, D., Corder, E. H., Dong, L.-M., Jakes, R., Alberts, M. J., Gilbert, J. R., Han, S.-H., Hulette, C., Einstein, G., Schmechel, D. E., Pericak-Vance, M. A., & Roses, A. D. (1994) *Exp. Neurol. 125*, 163−171.
Wetterau, J. R., Aggerbeck, L. P., Rall, S. C., Jr., & Weisgraber, K. H. (1988) *J. Biol. Chem. 263*, 6240−6248.
Whitson, J. S., Mims, M. P., Strittmatter, W. J., Yamaki, T., Morrisett, J. D., & Appel, S. H. (1994) *Biochem. Biophys. Res. Commun. 199*, 163−170.
Wisniewski, T., & Frangione, B. (1992) *Neurosci. Lett. 135*, 235−238.
Wisniewski, T., Castaño, E., Ghiso, J., & Frangione, B. (1993a) *Ann. Neurol. 34*, 631−633.
Wisniewski, T., Golabek, A., Matsubara, E., Ghiso, J., & Frangione, B. (1993b) *Biochem. Biophys. Res. Commun. 192*, 359−365.
Wisniewski, T., Castaño, E. M., Golabek, A., Vogel, T., & Frangione, B. (1994a) *Am. J. Pathol. 145*, 1030−1035.
Wisniewski, T., Ghiso, J., & Frangione, B. (1994b) *Neurobiol. Aging 15*, 143−152.
Wood, S. J., Chan, W., & Wetzel, R. (1996) *Biochemistry 35*, 12623−12628.
Yang, J. T., Wu, C. S. C., & Martinez, H. M. (1986) *Methods Enzymol. 130*, 208−269.

BI9624705